materials

MDPI

Article

Synthesis of New Complex Ferrite $Li_{0.5}MnFe_{1.5}O_4$: Chemical–Physical and Electrophysical Research

Mukhametkali Mataev [1], Altynai Madiyarova [1,*], Gennady Patrin [2], Moldir Abdraimova [1], Marzhan Nurbekova [1] and Zhadyra Durmenbayeva [1]

[1] Department of Chemistry, Faculty of Natural Sciences, Kazakh State Women's Teacher Training University, Almaty 050000, Kazakhstan; mataev_06@mail.ru (M.M.); abdraimova87@mail.ru (M.A.); nurbekova.0@qyzpu.edu.kz (M.N.); durmenbayeva@mail.ru (Z.D.)

[2] Department of General Physics, Siberian Federal University, Krasnoyarsk 660041, Russia; patrin@iph.krasn.ru

* Correspondence: madiyarova.altynai@mail.ru; Tel.: +7-702-660-29-92

Abstract: In this article, the sol–gel method was used as a synthesis method, which shows the physicochemical nature of the synthesis of a new complex material, ferrite $Li_{0.5}MnFe_{1.5}O_4$. The structure and composition of the synthesized ferrite were determined by X-ray phase analysis. According to analysis indicators, it was found that our compound is a single-phase, spinel-structured, and syngony-cubic type of compound. The microstructure of the compound and the quantitative composition of the elements contained within it were analyzed under a scanning electron microscope (SEM). Under a scanning electron microscope, microsystems were taken from different parts of $Li_{0.5}MnFe_{1.5}O_4$-type crystallite; the elemental composition of crystals was analyzed; and the general type of surface layer of complex ferrite was shown. As a result, given the fact that the compound consists of a single phase, the clarity of its construction was determined by the topography and chemical composition of the compound. As a result, it was found that the newly synthesized complex ferrites correspond to the formula $Li_{0.5}MnFe_{1.5}O_4$. The particles of the formed compounds have a large size (between 50.0 μm or 20.0 μm and 10.0 μm). Electrophysical measurements were carried out on an LCR-800 unit at intervals of 293–483 K and at frequencies of 1.5 and 10 kHz. An increase in frequency to 10 kHz led to a decrease in the value ε in the range of the studied temperature (293–483 K).

Keywords: sol–gel method; ferrites; X-ray; pycnometric density; elementary cell parameters; scanning electron microscope

check for updates

Citation: Mataev, M.; Madiyarova, A.; Patrin, G.; Abdraimova, M.; Nurbekova, M.; Durmenbayeva, Z. Synthesis of New Complex Ferrite $Li_{0.5}MnFe_{1.5}O_4$: Chemical–Physical and Electrophysical Research. *Materials* **2024**, *17*, 3754. https://doi.org/10.3390/ma17153754

Received: 4 June 2024
Revised: 1 July 2024
Accepted: 18 July 2024
Published: 30 July 2024

Copyright: © 2024 by the authors. Licensee MDPI, Basel, Switzerland. This article is an open access article distributed under the terms and conditions of the Creative Commons Attribution (CC BY) license (https://creativecommons.org/licenses/by/4.0/).

1. Introduction

Research in nanotechnology is a rapidly developing field at the forefront of physics and continues to be of particular interest to the scientific community [1]. Multifunctional materials, in particular, are studied for their effective properties combined in one smart compound [2,3]. A wide range of intelligent materials has been presented, and among them, significant attention has been paid to ferrites, which are considered promoter hosts due to their very prominent features [4,5].

Important results in this category of ceramics generally show excellent physicochemical properties, such as environmental mental health [6], chemical stability [7], high electrical resistance [8], and low price availability [9]. It is worth noting that in order for spinel ferrites to be useful for potential technological applications, a promising road was laid. Some prominent review articles indicate that the use of spinel ferrites for biomedical applications may be unavoidable due to their high biocompatibility [10] and low toxicity [6]. They have also been shown to have special properties for magnetic hyperthermia and magnetic resonance imaging [11,12]. Similarly, many discoveries have confirmed the development of this type of material as a suitable approach for ferrofluidic technology [13], wastewater treatment, catalysts [14], selective sun absorbers [15], and medical instruments [16].

With impressive properties such as conductivity, magnetic behavior, and high-temperature magnetic transition, mixed ferrites are soft ferrimagnetic compounds that show that they already exist in the field of technology. These materials are important due to their careless magnetization in room conditions [17,18].

The widespread use of spinel ferrites is due to their low price, easy preparation, and abundant use in technological and industrial applications [19]. The technological and industrial applications of these magnetic materials are due to their excellent electrical and magnetic properties, which leads to their use in magnetic memory devices, transformers, high-frequency applications, and electronic devices, such as mobile phones, camcorders, laptops, and computers [20].

Many researchers have studied the structural, electrical, and magnetic properties of various Li-based ferrites, such as Li-Mn [21], Li-Ni [22], Li-Co [23], Li-Mg [24], Li-Cr. [25], Li-Zn [26], and Li-Ti [27], which are manufactured by a ceramic method. However, ferrite prepared by the ceramic method involves the synthesis of high calcination temperatures to complete the solid-state reaction between the constituent oxides or carbonates, and the particles are obtained in significantly larger and uneven sizes. This leads to the formation of voids, and then low-density ferrites, when uneven particles are compacted. To overcome these difficulties, the sol–gel method is the preferred method for synthesizing nanoferrite on a volumetric scale by obtaining homogeneous particles, and the most convenient method for synthesizing nanoparticles. This is because of the simplicity of this method; the low-cost precursors; the fact that the annealing process is carried out in a short time; good control of the amount of crystallite; and other properties of materials [28].

Nanoscale manganese ferrites exhibit interesting structural and magnetic properties. They have a wide range of applications, from basic research to industrial applications. In this work, the composition of ferrite nanoparticles is studied.

2. Materials and Methods

The sol–gel method was used as an effective way to synthesize a new mixed ferrite of a complex mixed composition. In order to determine the composition of a new complex mixed ferrite obtained by the sol–gel method, an X-ray phase study was carried out, and in order to conduct quantitative and qualitative analysis, an examination under a scanning electron microscope and a study of electrophysical properties (dielectric conductivity and electrical resistance) were carried out.

As a primary raw material, distilled water of a manganese (III) oxide (“chemical pure”) brand, iron (III) oxide (“chemical pure”) brand, and lithium conbanate (“chemical pure”) brand were used. Trihydric alcohol–glycerin and citric acid were used as gel-forming reagents. The raw materials obtained by stoichiometric calculation were weighed on an analytical balance with a maximum accuracy of 0.0001 g, mixed, ground in an agate sieve, placed in an Alund crucible, and fired in a muffle furnace at a temperature of 1100 °C.

The resulting dried gel was fired in a muffle oven for 10 h at a temperature of 600 °C until a black powder was obtained. Finally, the resulting powder was fired in stages for 7 h at a temperature of 700–1100 °C in the air [29].

The pycnometric density of ferrites was determined by a previously described method [30]. Toluene and distilled water were used as indifferent liquids. The density of composite materials was measured five times, and the average values were calculated.

3. Results and Discussion

3.1. X-Ray Analysis

X-ray analysis was carried out at the Kazakh National Women’s Pedagogical University on a diffractometer Miniflex/600 (Rigaku. Almaty, Kazakstan). Analysis using a sika beam (U = 30 KV, J = 10 MA, rotation speed 1000 pulses per second, time constant t = 5 s, 2θ, with an angle interval between 5 and 900) was carried out on a Miniflex 600 RIGAKU, and filtered by a filter.

During the X-ray observation of the synthesized mixed complex ferrite, it was observed that the amorphous state of the samples decreased; the crystallization process was complete; and the kinetics of the sol–gel reaction were low. In addition, it is proved from the diffractogram shown in Figure 1 below that the samples changed from an amorphous state to a fully polycrystalline state, and the independent phase was completely formed.

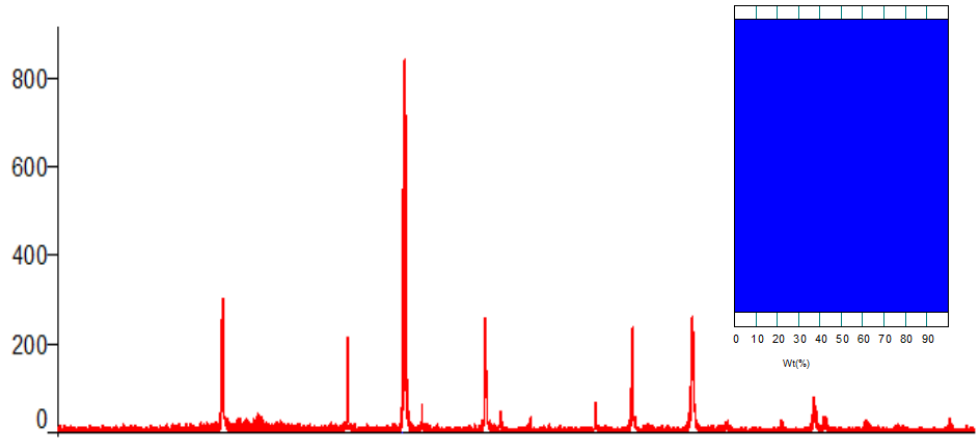


Figure 1. X-ray diffractogram of the complex ferrite $Li_{0.5}MnFe_{1.5}O_4$. Insert: phase ratio diagram.

Below are the results of the Rietveld method of indexing the diffractogram of the complex ferrite studied by X-ray analysis.

According to Scherrer's formula, the average size of crystallites can be written as follows:

$$d = \frac{K\lambda}{\beta \cos\theta} \quad (1)$$

where

d—average size of crystals;
K—dimensionless particle shape coefficient (Scherrer constant);
λ—wavelength of X-ray radiation;
β—half-height reflex width (2θ in radians and units);
θ—diffraction angle (Bragg angle).

A new complex mixed ferrite synthesized by the X-ray phase analysis method has the unit number Z = 8. $Li_{0.5}MnFe_{1.5}O_4$ is crystallized in a cubic wall-centered cell, and the space group is $Fd\bar{3}m$. Cell parameters: a = 8.3677, b = 8.3677, and c = 8.3677. The average size of crystallites according to Scherrer's formula through the X-ray wavelength of ferrite is 40.6 μm, and the correctness of the results of the X-ray studies was confirmed by the coincidence of the values of X-ray and pycnometric densities.

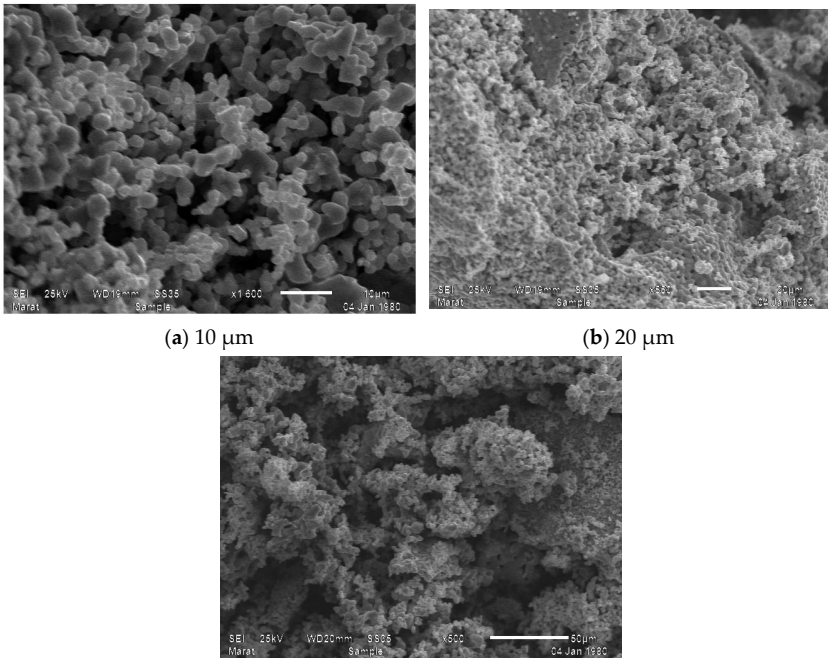
3.2. Scanning Electron Microscope Observations

The spectrum of the distribution of the element was studied by a scanning electron microscope (Sam) (Application Note team, Brooker, Berlin, Germany) in order to conduct quantitative and qualitative analysis, and study the percentage content of elements.

A scanning electron microscope (SEM) is designed to obtain a magnified image of an object by scanning it with an electron beam directed at it and recording the signal generated by the interaction of electrons with a detector. The small diameter of the probe, even at low accelerating voltages and high currents, allows for elemental analysis of samples with dimensions of the analyzed area of several tens of nanometers. The beam current detector is located on the microscope column below the aperture of the objective lens, so that the beam current can be monitored at any time during the analysis.

To study the morphology of the surface layer of samples of new complex mixed ferrite synthesized by the sol–gel method, an image of electric diffraction was studied using

an electron microscope scanning luminous microstructures. Electron monographs of the compound taken in an imaging electron microscope are given in Figure 2a–c.



(**a**) 10 μm (**b**) 20 μm

(**c**) 50 μm

Figure 2. Image of the new mixed complex ferrite $Li_{0.5}MnFe_{1.5}O_4$ measured with three different micrometer accuracies: (**a**) 10 μm; (**b**) 20 μm; (**c**) 50 μm.

The above images show the results of micrographs taken at magnifications of 10.0 μm, 20.0 μm, and 50.0 μm, and also show the general appearance of the complex ferrite surface layer. As a result, given that the compound consists of one phase, the clarity of its structure was determined by the topography and chemical composition of the compound. Figure 3 shows the spectrum patterns of the newly synthesized mixed complex ferrite $Li_{0.5}MnFe_{1.5}O_4$ and the elemental analysis results of the $Li_{0.5}MnFe_{1.5}O_4$ compound.

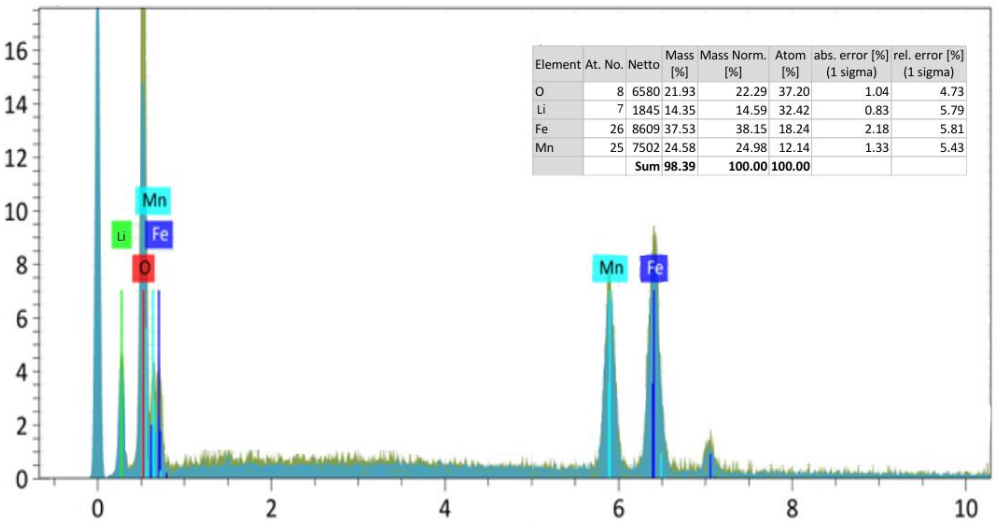


Figure 3. Spectrum samples of the $Li_{0.5}MnFe_{1.5}O_4$ compound. The results of the element analysis are built-in.

Based on the distribution map of elements, on the basis of solving the nature of crystallization, the chemical composition with microstructure and distribution zones of

chromium, iron, lithium, and oxygen atoms were studied. As a result of the numerical elemental composition study, it can be concluded that iron, chromium, lithium metals, oxygen, and carbon atoms are distributed in the 10.0 μm regions (Figure 2a). With an imaging electron microscope, it is possible to obtain nanoscale measurements of solids in powder form.

The spectrum of the distribution of the element was studied using a scanning electron microscope in order to conduct quantitative and qualitative analysis, and study the percentage content of elments. The spectrum samples of the synthesized new mixed complex ferrite and the results of the elemental analysis are shown in Figure 3.

3.3. Electrophysical Research

This was carried out according to methods of measuring electrophysical properties [31,32].

The study of electrophysical properties (dielectric constant and electrical resistance) was carried out by measuring the electrical capacitance of samples in the serial device LCR-800 (Taiwan) in thermostatic mode at an operating frequency of 1 kHz in continuous dry air, with holding time at each set temperature.

Samples parallel to the plane in the form of discs with a diameter of 10 mm and a thickness of 2–6 mm were pre-prepared with a binder mixture (1.5%). Pressing was carried out at a pressure of 20 kg/cm^2. The resulting discs were fired in the laboratory furnace "SNOL" at a temperature of 400 °C for 6 h. Then, they were carefully leveled on both sides.

The dielectric constant was determined from the electrical capacitance of the sample at certain values of the sample thickness and electrode surface. A Sawyer–Tower circuit was used to obtain the relationship between the electric induction d and the electric field strength E. Visual control of D (hysteresis loop e) was carried out on a C1-83 oscilloscope with a voltage divider consisting of a resistance of 6 Mom and 700 Kohm and a reference capacitor of 0.15 μF. The frequency of the generator was 300 Hz. In all temperature studies, samples were placed in a furnace; the temperature was measured with a chromium–aluminum thermocouple connected to a voltmeter B2-34 with an error of 0.1 MV. The temperature change rate was 5 K/min. The value of the dielectric constant at each temperature was determined by the following formula:

$$\varepsilon = \frac{C}{C_0} \tag{2}$$

where $C_0 = \frac{\varepsilon_0 \cdot S}{d}$ is the capacitance of the capacitor without the test substance (air).

Calculation of the width of the forbidden zone (ΔE) of the substance under investigation was determined by the following formula:

$$\Delta E = \frac{2kT_1T_2}{0.43(T_2 - T_1)} \lg \frac{R_1}{R_2}, \tag{3}$$

where k is the Boltzmann constant equal to 8.6173303 $\times \cdot 10^{-5}$ eB·K^{-1}; R_1 is the resistance at T_1; and R_2 is the resistance at T_2.

To ensure the reliability of the data obtained, the dielectric constant of a standard substance, barium titanate $BaTiO_3$, was measured at frequencies equal to 1 kHz, 5 kHz, and 10 kHz. Table 1 below shows the results of measurements of the electrophysical characteristics of $BaTiO_3$.

As can be seen from the data in Table 2, the values of the dielectric constant 293 K at 1 kHz and 5 kHz correspond satisfactorily to its recommended value of 1400 ± 250. In addition, observed changes in the electrical conductivity of $BaTiO_3$ at all frequencies (1 kHz, 5 kHz, and 10 kHz) at 383 K correspond to its transition from the perovskite cubic phase Pm3m to the tetragonal (polar) ferroelectric phase with the space group P4mm [33–35].

Table 1. Symmetry type and unit cell parameters of $Li_{0.5}MnFe_{1.5}O_4$.

Sample	**$Li_{0.5}MnFe_{1.5}O_4$**
Space group	$Fd\bar{3}m$, cubic side centered
Z	8
Parameter cell (Å)	8.3677(9)
a=	8.3677(9)
b=	8.3677(9)
c=	585.90(11)
V(A^3)	90
α	90
β	90
γ	40.6 μm
Average size of crystallites according to Scherrer's formula	
X-ray density (g/cm^3)	4.678
Pycnometric density (g/cm^3) *	4.675

* Calculated manually by pycnometer.

Table 2. Dependence of electrical resistance (R), electrical capacity (C), and dielectric constant (ε) on $BaTiO_3$ temperature.

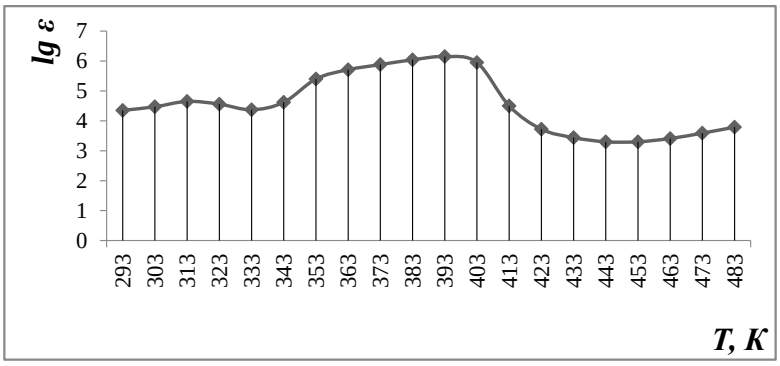
T, K	**C, nF**	**R, O_M**	**ε**	**lgε**	**lgR**
Measurement frequency at 1 kHz					
293	0.27278	13,400	1296	3.11	4.13
303	0.27426	13,270	1303	3.11	4.12
313	0.27715	12,910	1316	3.12	4.11
323	0.28125	12,560	1336	3.13	4.10
333	0.28772	11,890	1367	3.14	4.08
343	0.29313	11,210	1392	3.14	4.05
353	0.29916	10,290	1421	3.15	4.01
363	0.30751	9383	1461	3.16	3.97
373	0.31202	8831	1482	3.17	3.95
383	0.31702	9061	1506	3.18	3.96
393	0.32255	8814	1532	3.19	3.95
403	0.32967	7881	1566	3.19	3.90
413	0.3423	7098	1626	3.21	3.85
423	0.35119	6902	1668	3.22	3.84
433	0.36668	6153	1742	3.24	3.79
443	0.38018	6317	1806	3.26	3.80
453	0.39802	6010	1891	3.28	3.78
463	0.4169	5584	1980	3.30	3.75
473	0.43147	5149	2050	3.31	3.71
483	0.45456	4656	2159	3.33	3.67
Measurement frequency at 5 kHz					
293	0.25678	29,630	1220	3.09	4.47
303	0.2683	21,650	1274	3.11	4.34
313	0.2775	13,080	1318	3.12	4.12
323	0.28638	5236	1360	3.13	3.72
333	0.29667	4301	1389	3.14	3.63
343	0.30226	4733	1409	3.15	3.68
353	0.30787	3296	1436	3.16	3.52
363	0.31283	2966	1462	3.17	3.47
373	0.31843	2805	1486	3.17	3.45
383	0.32148	2529	1513	3.18	3.40
393	0.32578	2669	1527	3.18	3.43
403	0.32976	3172	1547	3.19	3.50
413	0.33303	4434	1566	3.19	3.65
423	0.33948	6377	1582	3.20	3.80
433	0.35613	9644	1613	3.21	3.98
443	0.3713	11,520	1692	3.23	4.06
453	0.3925	10,430	1764	3.25	4.02
463	0.41682	8021	1864	3.27	3.90
473	0.44245	5978	1980	3.30	3.78
483		3799	2102	3.32	3.58

Table 2. *Cont.*

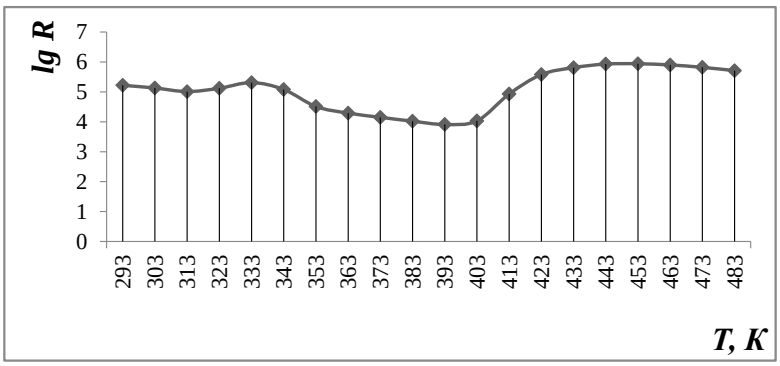
T, K	C, nF	R, O_M	ε	lgε	lgR
Measurement frequency at 10 kHz					
293	0.11814	152,300	561	2.75	5.18
303	0.18494	70,790	878	2.94	4.85
313	0.22927	32,200	1089	3.04	4.51
323	0.25954	11,870	1233	3.09	4.07
333	0.27501	4842	1306	3.12	3.69
343	0.28531	3312	1355	3.13	3.52
353	0.29302	2689	1392	3.14	3.43
363	0.29988	2257	1424	3.15	3.35
373	0.30652	1946	1456	3.16	3.29
383	0.31215	1689	1483	3.17	3.23
393	0.31667	1737	1504	3.18	3.24
403	0.32294	3130	1534	3.19	3.50
413	0.32779	5945	1557	3.19	3.77
423	0.33406	8231	1587	3.20	3.92
433	0.34256	8805	1627	3.21	3.94
443	0.35658	8052	1694	3.23	3.91
453	0.378	5967	1796	3.25	3.78
463	0.39475	4604	1875	3.27	3.66
473	0.41687	3343	1980	3.30	3.52
483	0.44203	2353	2100	3.32	3.37

It should be noted that despite the decrease in the values of the dielectric constant of $BaTiO_3$ at a frequency of 10 kHz, and at T equal to 293 K, 303 K, and 313 k, and all values of ε $BaTiO_3$ at all three frequencies (1 kHz, 5 kHz, and 10 kHz) in the range of 313–483 K, there are values up to about 2150, indicating that this frequency change does not particularly affect the temperature dependence of the dielectric constant. $BaTiO_3$ is in the range of 313–483 K.

Electrophysical measurements of $Li_{0.5}MnFe_{1.5}O_4$ in the range of 293–483 K and frequencies equal to 1, 5, and 10 kHz were carried out at the LCR installation (Table 3, Figure 4).



(**a**)



(**b**)

Figure 4. Dependence of dielectric constant (**a**) and electrical resistance (**b**) on temperature and frequency equal to 1 kHz.

Table 3. Dependence of electrical capacity (C), electrical resistance (R), and dielectric constant (ε) of material 2 on temperature and frequency.

T, K	C, nF	R, O_M	ε	lgε	lgR
Measurement frequency at 1 kHz					
293	7.7977	165,700	22,448	4.35	5.22
303	10.302	135,800	29,658	4.47	5.13
313	15.68	101,700	45,140	4.65	5.01
323	12.489	131,900	35,954	4.56	5.12
333	8.1684	203,600	23,515	4.37	5.31
343	14.516	121,200	41,789	4.62	5.08
353	86.933	32,510	250,266	5.40	4.51
363	176.65	19,300	508,547	5.71	4.29
373	265.14	14,110	763,295	5.88	4.15
383	378.56	10,520	1,089,813	6.04	4.02
393	495.27	8184	1,425,802	6.15	3.91
403	312.87	10,720	900,702	5.95	4.03
413	11.039	85,500	31,779	4.50	4.93
423	1.8105	379,400	5212	3.72	5.58
433	0.95809	649,900	2758	3.44	5.81
443	0.68585	843,600	1974	3.30	5.93
453	0.70009	874,900	2015	3.30	5.94
463	0.89737	796,100	2583	3.41	5.90
473	1.3483	666,100	3882	3.59	5.82
483	2.1329	511,600	6140	3.79	5.71
Measurement frequency at 5 kHz					
293	1.3926	140,100	4009	3.60	5.15
303	1.8886	115,400	5437	3.74	5.06
313	2.728	89,690	7853	3.90	4.95
323	1.517	128,100	4367	3.64	5.11
333	0.9064	184,900	2609	3.42	5.27
343	2.5719	93,070	7404	3.87	4.97
353	15.47	29,090	44,536	4.65	4.46
363	31.031	17,900	89,333	4.95	4.25
373	45.909	13,060	132,165	5.12	4.12
383	64.608	9799	185,996	5.27	3.99
393	82.944	7702	238,782	5.38	3.89
403	40.501	11,420	116,596	5.07	4.06
413	1.7403	79,660	5010	3.70	4.90
423	0.28075	293,500	808	2.91	5.47
433	0.13233	455,500	381	2.58	5.66
443	0.09429	533,500	271	2.43	5.73
453	0.09084	555,900	262	2.42	5.74
463	0.10483	536,400	302	2.48	5.73
473	0.13985	477,500	403	2.60	5.68
483	0.19866	401,900	572	2.76	5.60
Measurement frequency at 10 kHz					
293	0.62512	126,300	1800	3.26	5.10
303	0.85581	103,700	2464	3.39	5.02
313	1.188	83,510	3420	3.53	4.92
323	0.50394	127,500	1451	3.16	5.11
333	0.3238	169,200	932	2.97	5.23
343	1.2082	76,460	3478	3.54	4.88
353	7.2162	26,640	20,774	4.32	4.43
363	14.584	16,680	41,985	4.62	4.22
373	21.676	12,440	62,402	4.80	4.09
383	30.192	9304	86,918	4.94	3.97
393	39.355	7426	113,297	5.05	3.87
403	14.483	12,940	41,694	4.62	4.11
413	0.64942	83,960	1870	3.27	4.92
423	0.12128	243,700	349	2.54	5.39
433	0.06145	329,700	177	2.25	5.52
443	0.04865	351,900	140	2.15	5.55
453	0.04694	362,500	135	2.13	5.56
463	0.05137	360,400	148	2.17	5.56
473	0.06369	339,200	183	2.26	5.53
483	0.08415	306,100	242	2.38	5.49

The data in Table 3 and Figure 4 show that the value of the dielectric constant (ε) reaches a maximum value at 383 K, which is equal to 1.43·106 (1 kHz). Then, it decreases

to 6140 at 483 K (frequency 1 kHz). Increasing the frequency to 5 and 10 kHz leads to a decrease in ε in the entire temperature range under study (293–483 K).

The study of the temperature dependence of electrical resistance shows the complex nature of conductivity: at ΔT = 293–313 K—semiconductor, at ΔT = 313–333 K—metallic, at 333–393 K—semiconductor, at ΔT = 393–453 K—metallic, and at ΔT = 453–483 K—again, semiconductor.

The band spacing of 2 materials AT ΔT = 293–313 K (Table 4) and 333–393 K (Table 5) is equal to 1.91 and 1.19 EV (narrowband semiconductor), respectively, and AT ΔT = 453–483 K (Table 6) is equal to 3.04 EV (broadband semiconductor).

Table 4. Calculation of the width of the forbidden zone (ΔE) in the range 293–313 K.

T, K	lg R
293	5.22
313	5.01
$\Delta E = \frac{2\times0.000086173\times293\times313}{0.43(313-293)}\lg\frac{5.22}{5.01} = 1.91$эВ	

Table 5. Calculation of the width of the forbidden zone (ΔE) in the range 333–393 K.

T, K	lg R
333	5.31
393	3.91
$\Delta E = \frac{2\times0.000086173\times333\times393}{0.43(393-333)}\lg\frac{5.31}{3.91} = 1.19$эВ	

Table 6. Calculation of the width of the forbidden zone (ΔE) in the range 453–483 K.

T, K	lg R
453	5.94
483	5.71
$\Delta E = \frac{2\times0.000086173\times453\times483}{0.43(483-453)}\lg\frac{5.94}{5.71} = 3.04$ эВ	

4. Conclusions

Summing up the results of the study, a new mixed complex ferrite with the composition $Li_{0.5}MnFe_{1.5}O_4$ was synthesized for the first time by the sol–gel method. In order to determine the composition of the resulting new complex mixed ferrite, an X-ray phase study was carried out, and in order to conduct quantitative and qualitative analysis, an examination under a scanning electron microscope and a study of electrophysical properties (dielectric conductivity and electrical resistance) were carried out.

For the first time, syngony types and parameters of elementary cells of a complex mixed ferrite synthesized by the method of X-ray phase analysis were determined. $Li_{0.5}MnFe_{1.5}O_4$ (cubic, a = 8.3677(9), B = 8.3677(9), C = 8.3677(9) Å, Z = 8, denX-ray = 4.678 g/cm^3, denPycno = 4.675 g/cm^3); through the X-ray wavelength of ferrite, the average size of crystallites according to Scherrer's formula is 40.6 μm. The results of radiographic research showed that the synthesized compound is polycrystalline. The accuracy of crystallochemical data is evidenced by a satisfactory correspondence of X-ray and pycnometric densities.

Through a scanning electron microscope, microsystems were taken from different parts of $Li_{0.5}MnFe_{1.5}O_4$-type crystallite; the elemental composition of crystals was analyzed; and the general type of surface layer of complex ferrite was shown. As a result, given the fact that the compound consists of a single phase, the clarity of its construction was determined

by the topography and chemical composition of the compound. As a result, it was found that the newly synthesized complex ferrites correspond to the formula $Li_{0.5}MnFe_{1.5}O_4$. The particles of the formed compounds have a large size (between 50.0 μm or 20.0 μm and 10.0 μm). The results of the elemental analysis were presented in the form of a table.

Electrophysical measurements of $Li_{0.5}MnFe_{1.5}O_4$ on the LCR-800 unit were carried out at intervals of 293–483 K and frequencies of 1.5 and 10 kHz.

Given the fact that 293 K is equal to a relatively high value of 2.69 × 105 at 1 kHz, the maximum value of 383 K reached 1.43 × 106. Next, it was reduced to 6140 at 483 K (frequency of 1 kHz). An increase in frequency to 5 and 10 kHz led to a decrease in the entire test temperature interval (293–483 K).

The study of the dependence of electrical resistance on temperature shows the complex nature of conductivity: t = 293–313 K—semiconductor, t = 313–333 K—metal, 333–393 K—semiconductor, t = 393–453 K—metal, and T = 453–483 K—semiconductor again.

In the future, I will study the temperature dependence and magnetic sensitivity of the magnetization of synthesized complex ferrite in various magnetic fields.

Author Contributions: Conceptualization, A.M.; methodology, M.A., Z.D., G.P. and M.N.; formal analysis, M.N. and G.P.; resources, M.A., M.M. and Z.D.; writing—original draft preparation, A.M. and M.M. All authors have read and agreed to the published version of the manuscript.

Funding: This research received no external funding.

Institutional Review Board Statement: Not applicable.

Informed Consent Statement: Not applicable.

Data Availability Statement: Data are contained within the article.

Conflicts of Interest: The authors declare no conflict of interest.

References

1. Hossain, M.D.; Jamil, A.T.M.K.; Hossain, M.S.; Ahmed, S.J.; Das, H.N.; Rashid, R.; Khan, M.N.I. Investigation on structure, thermodynamic and multifunctional properties of Ni–Zn–Co ferrite for Gd3+ substitution. *RSC Adv.* **2022**, *12*, 4656. [CrossRef] [PubMed]
2. Gonçalves, J.M.; Silva, M.N.; Naik, K.K.; Martins, P.R.; Rocha, D.P.; Nossol, E.; Rout, C.S. Multifunctional spinel $MnCo_2O_4$ based materials for energy storage and conversion: A review on emerging trends, recent developments and future perspectives. *J. Mater. Chem.* **2021**, *9*, 3095. [CrossRef]
3. Yao, C.; Ismail, M.; Hao, A.; Thatikonda, S.K.; Huang, W.; Qin, N.; Bao, D. Annealing atmosphere effect on the resistive switching and magnetic properties of spinel Co_3O_4 thin films prepared by a sol–gel technique. *RSC Adv.* **2019**, *9*, 12615. [CrossRef] [PubMed]
4. Chandel, M.; Moitra, D.; Makkar, P.; Sinha, H.; Hora, H.S.; Ghosh, N.N. Synthesis of multifunctional $CuFe_2O_4$–reduced graphene oxide nanocomposite: An efficient magnetically separable catalyst as well as high performance supercapacitor and first-principles calculations of its electronic structures. *RSC Adv.* **2018**, *8*, 27725. [CrossRef] [PubMed]
5. Li, Z.; Wang, Z.L.; Wang, Z. In situ tuning of crystallization pathways by electron beam irradiation and heating in amorphous bismuth ferrite films. *RSC Adv.* **2018**, *8*, 23522. [CrossRef] [PubMed]
6. Malima, N.M.; Khan, M.D.; Choi, J.; Gupta, R.K.; Mashazi, P.; Nyokong, T.; Revaprasadu, N. Solventless synthesis of nanospinel $Ni_{1-x}Co_xFe_2O_4$ ($0 \leq x \leq 1$) solid solutions for efficient electrochemical water splitting and supercapacitance. *RSC Adv.* **2021**, *11*, 31002. [CrossRef] [PubMed]
7. Jangam, K.; Patil, K.; Balgude, S.; Patange, S.; More, P. Magnetically separable $Zn_{1-x}Co_{0.5x}Mg_{0.5x}Fe_2O_4$ ferrites: Stable and efficient sunlight-driven photocatalyst for environmental remediation. *RSC Adv.* **2020**, *10*, 42766. [CrossRef] [PubMed]
8. Bastianello, M.; Gross, S.; Elm, M.T. Thermal stability, electrochemical and structural characterization of hydrothermally synthesised cobalt ferrite ($CoFe_2O_4$). *RSC Adv.* **2019**, *9*, 33282. [CrossRef] [PubMed]
9. Kobylinska, N.; Klymchuk, D.; Shakhovsky, A.; Khainakova, O.; Ratushnyak, Y.; Duplij, V.; Matvieieva, N. Biosynthesis of magnetite and cobalt ferrite nanoparticles using extracts of "hairy" roots: Preparation, characterization, estimation for environmental remediation and biological application. *RSC Adv.* **2021**, *11*, 26974. [CrossRef]
10. Pham, T.N.; Huy, T.Q.; Le, A.T. Spinel ferrite (AFe_2O_4)-based heterostructured designs for lithium-ion battery, environmental monitoring, and biomedical applications. *RSC Adv.* **2020**, *10*, 31622. [CrossRef]
11. Manohar, A.; Chintagumpala, K.; Kim, K.H. Mixed Zn–Ni spinel ferrites: Structure, magnetic hyperthermia and photocatalytic properties. *Ceram. Int.* **2021**, *47*, 7052. [CrossRef]

12. Kefeni, K.K.; Msagati, T.A.M.; Nkambule, T.T.I.; Mamba, B.B. Spinel ferrite nanoparticles and nanocomposites for biomedical applications and their toxicity. *Mater. Sci. Eng.* **2020**, *107*, 110314. [CrossRef] [PubMed]
13. Kharat, P.B.; Shisode, M.V.; Birajdar, S.D.; Bhoyar, D.N.; Jadhav, K.M. Synthesis and characterization of water based $NiFe_2O_4$ ferrofluid. *AIP Conf. Proc.* **2017**, *1832*, 050122. [CrossRef]
14. Taneja, S.; Thakur, P.; Ravelo, B.; Thakur, A. Nanostructured Rare Earth Nd^{3+} doped Nickel–Zinc–Bismuth Spinel Ferrites: Structural, Electrical and Dielectric Studies. *Mater. Res. Bull.* **2022**, *154*, 111937. [CrossRef]
15. Kim, J.H.; Kim, H.E.; Kim, J.H.; Lee, J.S. Ferrites: Emerging light absorbers for solar water splitting. *J. Mater. Chem. A* **2020**, *8*, 9447. [CrossRef]
16. Somvanshi, S.B.; Jadhav, S.A.; Khedkar, M.V.; Kharat, P.B.; More, S.D.; Jadhav, K.M. Hyperthermic evaluation of oleic acid coated nano-spinel magnesium ferrite: Enhancement via hydrophobic-to-hydrophilic surface transformation. *Ceram. Int.* **2020**, *46*, 13170. [CrossRef]
17. Nilar, L.; Fauzi, M.A.N.; Sreekantan, S.; Othman, R. Physical and electromagnetic properties of nanosized Gd substituted Mg–Mn ferrites by solution combustion method. *Phys. B Condens. Matter* **2015**, *461*, 134. [CrossRef]
18. XiuBo, X.; Wang, B.; Wang, Y.; Ni, C.; Sun, X.; Du, W. Spinel structured MFe_2O_4 (M = Fe, Co, Ni, Mn, Zn) and their composites for microwave absorption: A review. *Chem. Eng. J.* **2022**, *428*, 131160. [CrossRef]
19. Ahmad, I.; Farid, M.T. Characterization of cobalt based spinel ferrites with small substitution of gadolinium. *World Appl. Sci. J.* **2012**, *19*, 464. [CrossRef]
20. Fu, Y.P.; Lin, C.H.; Liu, C.W. Preparation and magnetic properties of $Ni_{0.25}Cu_{0.25}Zn_{0.5}$ ferrite from microwave-induced combustion. *J. Magn. Magn. Mater.* **2004**, *283*, 59. [CrossRef]
21. Ravinder, D.; Balachander, L.; Venudhar, Y.C. Electrical conductivity in manganese-substituted lithium ferrites. *Mater. Lett.* **2001**, *49*, 267. [CrossRef]
22. Trivedi, U.N.; Jani, K.H.; Modi, K.B.; Joshi, H.H. Study of cation distribution in lithium doped nickel ferrite. *J. Mater. Sci. Lett.* **2000**, *19*, 1271. [CrossRef]
23. Abo El Ata, A.M.; Attia, S.M.; El Kony, D.; Al-Hammadi, A.H. Spectral, initial magnetic permeability and transport studies of $Li_{0.5-0.5x}Co_xFe_{2.5-0.5x}O_4$ spinel ferrite. *J. Magn. Magn. Mater.* **2005**, *295*, 28. [CrossRef]
24. Ravinder, D.; Reddy, P.V.B. Thermoelectric power studies of polycrystalline magnesium substituted lithium ferrites. *J. Magn. Magn. Mater.* **2003**, *263*, 127. [CrossRef]
25. Laishram, R.; Prakash, C. Magnetic properties of Cr^{3+} substituted Li–Sb ferrites. *J. Magn. Magn. Mater.* **2006**, *305*, 35. [CrossRef]
26. Sattar, A.A.; El-Sayed, H.M.; Agami, W.R.; Ghani, A.A. Magnetic properties and electrical resistivity of Zr^{4+} substituted Li-Zn ferrite. *Am. J. Appl. Sci.* **2007**, *4*, 89–93. [CrossRef]
27. Surzhikov, P.; Pritulov, A.M.; Ivanov, Y.F.; Shabardin, R.S.; Usmanov, R.U. Electron-Microscopic Study of Morphology and Phase Composition of Lithium-Titanium Ferrites. *Russ. Phys. J.* **2001**, *44*, 420. [CrossRef]
28. Mataev, M.M.; Madiyarova, A.M.; Patrin, G.S.; Abduraimova, M.R.; Nurbekova, M.A.; Tursunova, Z.I. Synthesis and physico—Chemical characteristics of complex ferrite $CrNaFe_2O_5$. *Chem. J. Kaz.* **2024**, *1*, 109–118. [CrossRef]
29. Mataev, M.M.; Mustafin, E.S.; Kasenov, R.Z.; Pudov, A.M.; Kaikenov, D.A.; Bogzhanova, Z.K. X ray Diffraction Study of the $YbM^{II}Fe_5O_{12}$ (MII = Mg, Ca, Sr) Ferrites. *Inorg. Mater.* **2014**, *50*, 622–624. [CrossRef]
30. Mataev, M.M.; Abdraimova, M.R.; Saxena, S.X.; Nuketaeva, D.Z.; Zheksembieva, B.T. Syntesis and X-ray analysis of complex ferrites. *Key Eng. Mater.* **2017**, *744*, 393–398. [CrossRef]
31. Okazaki, K. *Technology of Ceramic Dielectrics*; Energiya: Moscow, Russia, 1976; 256p.
32. Kasenov, B.K.; Kasenova, S.B.; Sagintaeva, Z.I.; Baisanov, S.; Lu, N.Y.; Nukhuly, A.; Kuanyshbekov, E.E. Heat Capacity and Thermodynamic Functions of Titanium-Manganites of Lanthanum, Lithium and Sodium of $LaLi_2TiMnO_6$ and $LaNa_2TiMnO_6$. *Molecules* **2023**, *28*, 5194. [CrossRef] [PubMed]
33. Fesenko, E.G. *The Perovskite Family and Ferroelectricity*; Atomizdat: Moscow, Russia, 1972.
34. Venevtsev, Y.N.; Politova, E.D.; Ivanov, S.A. *Ferroelectric and Antisegnetoelectrics of the Barium Titanate Family*; Chemistry: Moscow, Russia, 1985.
35. Lines, M.; Glass, A. *Ferroelectrics and Related Materials*; Mir: Moscow, Russia, 1981.

Disclaimer/Publisher's Note: The statements, opinions and data contained in all publications are solely those of the individual author(s) and contributor(s) and not of MDPI and/or the editor(s). MDPI and/or the editor(s) disclaim responsibility for any injury to people or property resulting from any ideas, methods, instructions or products referred to in the content.